Chapter 1

GENERAL INTRODUCTION, SCOPE AND CONTENTS OF PRESENT WORK

This chapter gives the description of experimental methods employed in the preparation and characterization of $PbO-Sb_2O_3-As_2O_3$ glasses and glass ceramics. The details of the apparatus used and the techniques adopted for measuring dielectric properties, optical absorption, IR, Raman, ESR, photo luminescence spectra and magnetic susceptibility are also described in detail in this chapter

General introduction Scope and Contents of present work

1.2 Introduction

Glass is an inorganic solid material that is usually clear or translucent with different colors. It is hard, brittle and stands up to the effects of wind, rain or Sun. In more precise terminology, glass is an amorphous solid completely lacking in long range, periodic atomic structure and exhibiting a region of glass transformation behavior. Any material, inorganic, organic or metallic, formed by any technique, which exhibits glass transformation behavior, is a glass.

The exceptionally rapid development of technological research in all fields of knowledge is accompanied by intense work by scientists and technologists on glass materials. These materials have potential applications as laser materials, IR domes, optical fibers, modulators, memory devices, photonic devices for communication and advanced computer applications and as semi conducting devices. Applications of these materials can also be found in nuclear waste management, optical fibers, solid electrolytes, electronic displays, biocompatible implants, dental posterior materials, high performance composites etc. In view of such vast and diversified applications, the investigation on the development and characterization of different glass materials has gained momentum in the recent years.

Unlike crystals, glass materials do not possess the long-range periodicity of the arrangement of the atoms. These materials possess ionic as well as covalent bonding interaction. According to Zachariasen [1] there are only five oxide materials which form the glass by themselves viz., SiO_2, GeO_2, B_2O_3, As_2O_3 and P_2O_5; two more non-oxide compounds viz., As_2S_3 and BeF_2 are also added to this list recently [2]. Though, the glass materials do not possess the long-range periodicity but they retain short range order with AO_3 and AO_4 basic building blocks and follow certain rules proposed by Zachariasen. Basing on these rules, a continuous random network for a glass can be constructed as shown in Fig. 1.1.

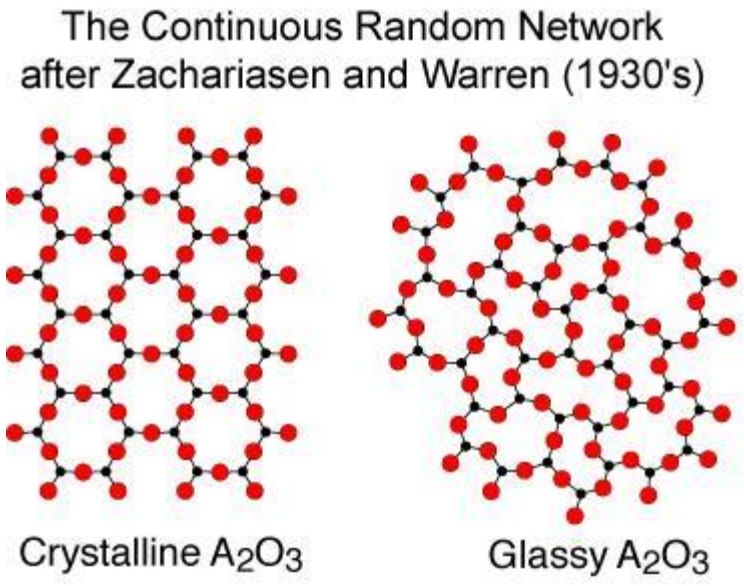

Fig. 1.1 Two dimensional schematic of crystalline and non-crystalline (glass) materials.

As per these rules, the oxides of the type AO (CaO, BaO etc.), A_2O (Li_2O, Na_2O etc.) can not form glasses on their own and the rules are satisfied only for oxides of the type A_2O_3, AO_2 and A_2O_5 and for non-oxide compounds As_2S_3 and BeF_2. The cations such as A^+ (example Li^+, Na^+, K^+ etc.,) A^{2+} (example Ca^{2+}, Pb^{2+}, Cd^{2+} etc.,) other than A^{3+} and A^{4+} are known as network modifiers. Alkali oxides/fluorides, alkali earth oxides/fluorides, ZnO, PbO, CdO etc., are some of the basic examples of modifiers in glass network. These modifiers break-up the continuous network by introducing non-bridging oxygens (Fig.1.2).

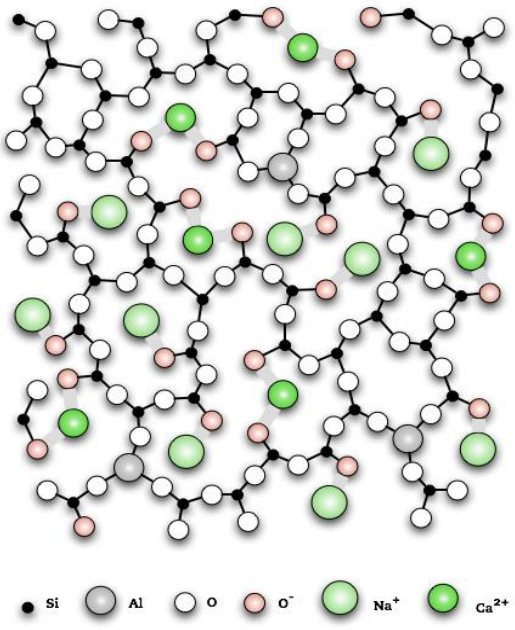

Fig. 1.2 Structure of a glass with modifier oxides

A third group of oxides known as intermediate class of oxides also exist which by themselves not readily form glasses but do so when mixed with other oxides; such oxides are known as intermediate glass formers. The examples of this group include Sb_2O_3, Al_2O_3, Ga_2O_3, In_2O_3, TeO_2, WO_3, MoO_3, V_2O_5 etc.

The summary of the rules for glass formation proposed by Zachariasen is as follows:

a) A high proportion of glass network forming cations (Si, B, P, Ge, As, etc.,) is surrounded by oxygen tetrahedra or triangles.
b) The polyhedra, share should not more than one corner with each other
c) The number of corners of polyhedra is less than 6
d) Anions (O^{2-}, S^{2-}, F^-) should not be linked with more than two cations and do not form additional bonds with any other cations.
e) At least three corners of polyhedra must connect with the neighboring polyhedra.
f) The network modifiers participate in the glass network with the co-ordination number generally greater than 6.
g) Intermediate glass formers (do not form the glass on their own) but either reinforce network or loosen the network with co-ordination

number 6 to 8 and may participate in the network with coordination number 3 or 4 in the presence of modifiers.

Excellent reviews and articles on the topology of the glass by Vogel [2], Elliott [3], Polk [4], Rao [5], Ingram [6] and Shelby [7] give useful information.

Glasses are traditionally formed by cooling the molten liquid. However, there are a number other non-conventional methods like chemical vapour deposition, solgel process techniques, etc. When a liquid is cooled from high temperature, crystallization may take place at the melting point T_m. If the crystallization takes place, there will be abrupt change in the volume/enthalpy at T_m. Continued cooling of the crystal will result in a further decrease in the volume/enthalpy due to the heat capacity of the crystal. If the liquid is cooled below the melting temperature without crystallization, a super cooled liquid is obtained. In this region, the structure of the liquid continues to rearrange as the temperature decreases, but there is no abrupt decrease in volume/enthalpy due to discontinuous structural rearrangement.

As the liquid is cooled further, the viscosity increases. This increase in viscosity eventually becomes so great that the atoms can no longer completely rearrange to the equilibrium liquid structure, during the time

allowed by the experiment. The structure begins to lag behind that which would be present if sufficient time were allowed to reach equilibrium. The enthalpy begins to deviate from the equilibrium line, following a curve of gradually decreasing slope, until it eventually becomes determined by the heat capacity of the frozen liquid, *i.e.*, the viscosity becomes so great that the structure of the liquid becomes fixed and is no longer temperature-dependent. The temperature region lying between the limits where the enthalpy is that of the equilibrium liquid and that of the frozen solid, is known as the glass transformation region. The frozen liquid is now a glass. The glass transition temperature lies in between these two temperatures, as such it is a fictious temperature and depend on the heating rate and previous thermal history of the sample.

This process of changes in volume/enthalpy with temperature as a super cooled liquid is cooled through the glass transition region is illustrated in Fig. 1.3.

During the last few decades a variety of inorganic glasses have been developed with an attempt to achieve suitable electrical, mechanical and optical characteristics. These characteristics are associated with the improved physical properties such as electrical resistance, mechanical strength, glass transparency, IR transmission performance and their ability to accept more

transition/rare earth metal ions for their use in solid-state devices. Work along these lines was carried out on a number of glasses giving valuable information [8-13]. Investigations on electrical properties such as dielectric properties of glasses help to have an idea over their insulating character. Investigations on the spectroscopic properties such as optical absorption, infrared spectra and electron spin resonance can be used as probes to throw some light on the structural aspects of these glasses. Studies on fluorescence spectra especially rare earth doped glasses will help to asses the suitability of the glasses for laser materials.

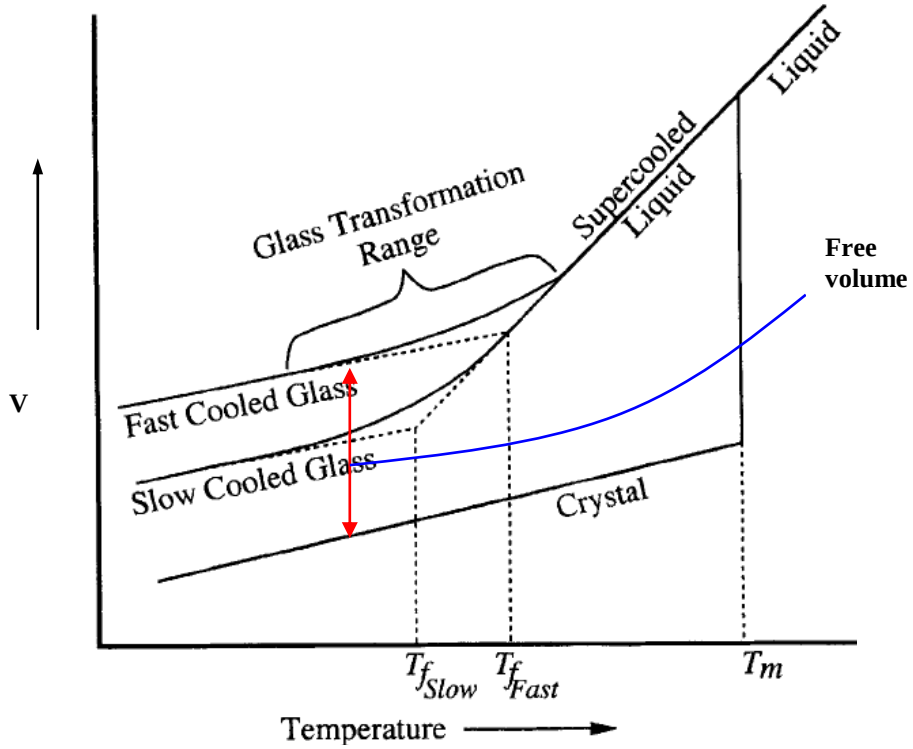

Fig. 1.3 Schematic illustration of the change in volume with temperature as super cooled liquid is cooled through the glass transition temperature T_g.

Glass-ceramics

Glass-ceramic processing consists of melting together a mixture of compounds (usually oxides), to form a fluid of high viscosity, which when cooled at moderate rates gradually increase in viscosity until a vitreous (non-crystalline) solid (glass) is formed; as has been discussed above. The cooled glass body is then partially or completely crystallized (devitrified) by heat treatment. A distinctive advantage of the glass-ceramic process is that crystallization may be accomplished at a temperature where the viscosity of the glass is still high, so that the glass body does not deform, but to a first approximation, passes from a solid glass shape to a solid crystal-line shape of the same dimensions.

In these materials finely dispersed crystalline structures are stimulated to "grow" within the solidified glass matrix by a process of controlled devitrification. The presence of native crystalline inclusions (Fig. 1.4) strengthens the glass and makes it more flexible, reducing the presence and severity of micro-cracks and acting as crack stoppers. Further, glass ceramics materials posses more mechanical strength even at high temperatures than that of glasses.

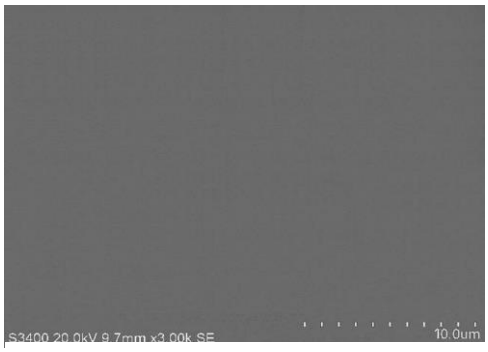

Fig. 1.4(a) SEM picture of a glass before crystallization

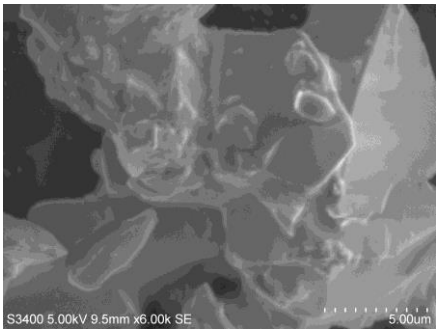

Fig. 1.4(b) SEM picture of a glass after crystallization

The advantages of the glass ceramic process have been applied to a whole spectrum of compositions and applications. Their high mechanical strength and chemical inertness makes them suitable for prosthetic implants, for missile radomes. Yet, their low thermal expansion coefficients, makes these materials suitable for gas tight electrical feedthroughs. These materials are very poor conductors of electricity. It is also well established that the crystallization of the glasses influences the optical properties to a greater extent.

Most glass ceramic formulations contain small amounts of special additives, called nucleating agents (catalysts or mineralizers) that initiate the crystallization process and influence the particular mix of phases that develops. Platinum, TiO_2, ZrO_2, CoO, MnO, NiO, V_2O_5, Fe_2O_3, Ag_2O, etc., from 0.01 to 10 percent are commonly used nucleating agents in glass-ceramics. Additionally, some fluorides and phosphates can also be

considered as nucleating agents but these additives primarily enhanced the phase separation, while the above mentioned compounds are soluble in the glass, but they precipitate at reduced temperatures.

Although the nucleation and growth process in glass ceramics has been extensively studied for the last five decades, at present there is no unambiguous general theory that explains how the nucleating agents operate. Most available models are specific to a given system and they commonly postulate the formation of some sort of heterogeneity by the nucleating agent that catalyzes the subsequent crystallization [2, 14].

Recently, the nucleation and crystal growth mechanism in a variety of glass materials that include lithium aluminium silicates, zirconium magnesium silicate, sodium potassium silicates, calcium phosphate etc., has been studied in detail [2, 15].

There are two parts to the creaming process; crystal nucleation and crystal growth. Each phase happens because the glass body is held at a specific temperature for a specific length of time.

Crystals have a tendency to develop in a mixture of glass when it is held at a specific temperature, called the crystal nucleation temperature. This means that when held at the crystal nucleation temperature, multiple seed crystals begin to grow throughout the glass body. The longer the glass is

held at this temperature, the more seed crystals will form. Ideally, a glass ceramic will be strongest when there are a very large number of small crystals distributed evenly throughout its mass. Once a seed crystal forms, it will also begin growing larger at this temperature, but quite slowly. If the temperature of the glass body is held at the crystal nucleation temperature for a very long time, a very large number of crystals of widely varying size will form. The earliest to seed will be the largest while the crystals that have recently just begun to grow will be the smallest.

In order to better control the esthetics of the finished product, the ideal glass ceramic will have crystals of a small, relatively uniform size. Any form of devitrification in a glass structure will produce one degree or another of opacity. Large crystals are more prone to making the glass opaque, while small crystals evenly scattered throughout the structure have less of an impact on the optical qualities of the finished product. Thus it is of benefit to hold the temperature at the point of maximum seeding for a finite length of time in order to allow numerous tiny seed crystals to nucleate, and then to stop the nucleation process and encourage the ones that have already formed to grow to suitable size.

1.3 Scope of the present work

Antimony oxide is a white powder and is derived from the mineral stibnite or produced by the oxidation of antimony metal or as a byproduct of the refining or antimonial-lead alloys. In the vapour and in the solid below 570 ^{o}C it consists of Sb_4O_6 type molecules; the high temperature solid form is highly polymeric. The oxide of antimony is valuable for its high 'tinctorial strength' (hiding power or opacity) when used in conjunction with halogen-containing compounds. It has very high surface catalytic activity, can be used as an accelerant in terylen polyester industry and in high-grade plastic, rubber, dye, fiber, insulation materials, chemical composite materials, etc. Earlier, the glass industry used antimony as a decolorizing and fining agent to clarify glasses and as a stabilizing agent in the production of emerald green glass.

The Sb_2O_3 heavy metal oxide based glasses, have attracted extensive investigation in recent years; these glasses posses large non-linear optical susceptibility (χ^3) coefficient [16] that makes them suitable for potential applications in non-linear optical devices (such as ultrafast optical switches and power limiters), broad band optical amplifiers operating around 1.5 μ.m [17-20] and in a number of solid state ionic devices. Antimony oxide participates in the glass network with SbO_3 structural units and can be

viewed as tetrahedrons with the oxygen at three corners and a lone pair of electrons of antimony (Sb^{3+}) at the fourth corner localized in the third equatorial direction of Sb atom (Fig.1.5); the deformability of this pair probably could make these glasses to exhibit non – linear optical susceptibility [21]. Further, Sb_2O_3 based glasses are known due to their significant transmission potential in the infrared region and possess high refractive index [22-24]. Attempts were made to improve the physical characteristics of these glasses by the addition of alkali oxides (like Li_2O), alkali halides (like NaCl, NaI) and alkali sulphides (like Na_2S, K_2S) to Sb_2O_3 glass matrices [18, 25-27] to a considerable extent. The antimony oxide as such is an incipient glass network former which does not form glass on its own.

PbO is an interesting modifier oxide that is in the present glass matrix. It acts both as modifier and network former with [$PbO_{4/2}$] pyramidal units connected in puckered layers; participates in the glass network with covalent and ionic bindings.

Earlier, arsenic oxide was used as a fining agent in glasses, where it helps to remove the bubbles. As_2O_3 containing glasses were identified as the low loss materials for long distance optical transmission. These glasses containing As_2O_3 were found to exceptionally high Raman scattering

coefficients and considered to be suitable for active fiber Raman amplification. Further, As_2O_3 is the only strong glass former besides GeO_2 having significant transmission potential farther into the infrared. This is illustrated by calculated wavelength of $\lambda_{o,}$ the material dispersion crossover point, which is 1.3 μm for P_2O_5, B_2O_3 and SiO_2, 1.7 μm for GeO_2 and 1.9 μm for As_2O_3.

As_2O_3 is the most important oxide of arsenic and is obtained by burning air [28, 29] or by the hydrolysis of $AsCl_3$ [30]. The basic structural unit in As_2O_3 at temperatures below 800 ^{0}C is the AsO_3 pyramid. In the vapour phase below 800 ^{0}C four AsO_3 units share (oxygen) corners to form the As_4O_6 molecule as illustrated in Fig. 1.6 [31, 32]. An alternating way of the viewing the molecule as a tetrahedral As_4 molecule with each As-As bond replicated by an As-O-As bridging oxygen atom, oxygen atoms being arranged at the vertices of a regular octahedron.

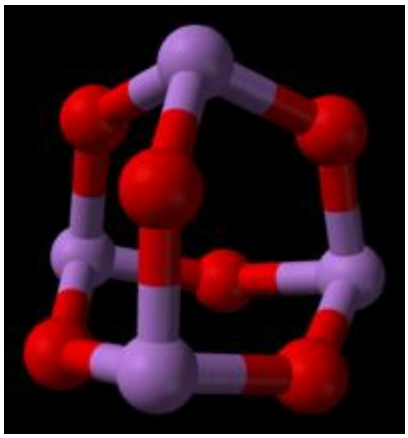

Fig. 1.6 Molecular structure of As_4O_6

Solid As_2O_3 is an interesting material in that it exists in the crystalline state as both a molecular solid (arsenolite) and as two polymorphs having an infinite layer structure (claudetite I and II). Arsenolite is formed by vapour deposition below 250 ^{0}C [30] or by crystallization from an aqueous or hydrochloric acid solution of As_2O_3 [28, 29]. In either case the formation is dominated by kinetic factors since the claudetite is the thermodynamically stable phase [33]. The structure of arsenolite is same to that of diamond with each carbon atom is replaced by an As_2O_6 molecule, the molecule on two sub lattices being rotated by π/2 relative to each other [34]. As_2O_3 is a strong network former with corner sharing AsO_3 pyramids; earlier neutron diffraction studies indicate that normal bond length of As-O lie between 1.72 – 1.81 ^{o}A and As-O-As bond angles lie in the range 90-103^o and 123-135^o respectively [35].

Though As_2O_3 seems to be a very efficient network former [36-39], but for a literature survey it is apparent that there are only few studies on As_2O_3 glass system, presently due to difficulties which appear in the preparations of these glasses.

The optical transparency of PbO-Sb_2O_3 glasses can further be improved in the blue region by replacing a part of Sb_2O_3 by As_2O_3 [40].

As_2O_3 is a strong network former [41] and is found to affect the far infrared transmission of Sb_2O_3 glasses to a less extent, since the frequencies of some of the fundamental modes of vibration of As_2O_3 structural groups lie in the region of vibration of SbO_3 structural groups [42]. Moreover, it is also expected that AsO_3 groups form a single arsenic-antimony-oxygen framework with the Sb_2O_3 structural units and may strengthen its structure.

The characteristics of glass ceramic however depend on the kind and quantity of the crystal phase formed as well as on the residual glass composition. Hence, the selection of a suitable nucleating agent in the correct concentration and determination of the temperature and the time of nucleation and growth are important factors in the formation of a glass ceramic. The nucleating agents that are generally used for controlled crystallization processes, giving rise to enormous numbers of nucleation centres in the original glass are, gold, silver, platinum or the oxides of Ti, Cr, Mn, Ce, V, Ni and Zr or certain sulfides or fluorides. In the present study three interesting nucleating agents (viz., MoO_3, MnO and NiO) are chosen for inducing crystallization in these glasses. Additionally, the transition metal ions are very interesting ions to probe in the glass ceramic networks because their outer d-electron orbital functions have rather broad radial distributions and their responses to surrounding actions are very sensitive; as

a result these ions influence the physical properties of the glasses to a substantial extent.

Three series of elements are formed by filling the 3d, 4d and 5d shells of electrons. Together these comprise the d-block elements. They are often called ‘transition elements’ because their position in the periodic table is between s-block and p-block elements. Their properties are transitional between the highly reactive metallic elements of the s-block, which typically form ionic compounds, and the elements of p-block, which are largely covalent. In s-and p-blocks, electrons are added to the outer shell of the atom where as in d-block they are added to the penultimate shell. Typically transition elements have an incompletely filled d level.

In the d-block elements, the penultimate shell of electrons is expanding. Thus they have many physical and chemical properties in common and hence all the transition elements are metals. They are therefore good conductors of electricity and yet have a metallic luster and are hard, strong and ductile. They also form alloys with other metals.

Table 1.1

Oxidation states of transition metal elements

	Sc	Ti	V	Cr	Mn	Fe	Co	Ni	Cu	Zn
Electronic Structure	d^1s^2	d^2s^2	d^3s^2	~~d^4s^2~~ d^5s^1	d^5s^2	d^6s^2	d^7s^2	d^8s^2	~~d^9s^2~~ $d^{10}s^1$	$d^{10}s^2$
Oxidation States	II	II	II	I II	II	II	II	I II	II	II
	III	III	III	III	III	III	III	III	III	
		IV	IV	IV	IV	IV	IV	IV		
			V	V	V	V	V			
				VI	VI	VI				
					VII					

One of the most striking features of the transition metal elements is that they usually exist in several different oxidation states (Table 1.1). Furthermore, the oxidation states change in units of one, e.g. Mo^{5+} and Mo^{6+}, Mn^{2+} and Mn^{3+}.

Among the first five transition metal elements, the correlation between the electronic structures and minimum and maximum oxidation states in simple compounds is complete. In the highest oxidation states of these first five elements, all of the s and d electrons are being used for bonding. Thus the properties depend only on size and valency, and consequently show some similarities with elements of the main groups in similar oxidation states. If

the d^5 configuration is exceeded, i.e. in the last five elements, the tendency for all the d electrons to participate in the bonding decreases.

The covalent radii of the elements decrease from left to right across a row in the transition series, until near the end when the size increases slightly. On passing from left to right, extra protons are placed in the nucleus and extra orbital electrons are added. The orbital electrons shield the nuclear charge incompletely (d electrons shield less efficiently than p electrons, which in turn shield less effectively than s electrons). Because of this poor screening by d electrons, the nuclear charge attracts all of the electrons more strongly: hence a contraction in size occurs.

Recently, much attention has been paid to research in inorganic glasses doped with transition metal ions because of their technological importance in the development of tunable solid state lasers, new luminescence materials, solar energy converters and fiber optic communication devices. In view of these, it is felt worthwhile to have some understanding over the dielectric and spectroscopic properties of $PbO{-}Sb_2O_3{-}As_2O_3$ glasses crystallized with three transition metal (viz., molybdenum, manganese and nickel) ions. The studies on dielectric properties and the dependence of these properties on the composition, structure and on various external factors such as humidity, radiation effect,

mechanical action etc., pave the way for estimating the insulating character. Whereas the investigations on spectroscopic (viz., optical absorption, electron spin resonance, infrared and photo luminescence spectra) properties give the information on environment and the oxidation states of the transition metal ions in the glass network and also help to assess the suitability of these glasses for practical applications.

A preliminary description of the above-mentioned properties along with their relation to some of the investigations (similar to those of present work) on $PbO-Sb_2O_3-As_2O_3$ glass ceramics is given below:

1.2.1 Physical parameters

Some physical parameters useful for characterization $PbO-Sb_2O_3-As_2O_3$ glass ceramics mixed with transition metal oxides are estimated from the measured value of density (d) and the average molecular weight $\overline{M}$, using the following equations [43-46]:

The transition metal ion concentration (N_i) is obtained from:

$$\text{(i) } N_i = \frac{N_A M(\text{mol}\%) d}{\overline{M}} \qquad (1.1)$$

From the N_i values obtained, the polaron radius (r_p) and inter – ionic distance (r_i) of transition metal ions could be evaluated:

$$\text{(ii)}\quad \text{Inter – ionic distance } r_i\ (\text{Å}) = \left[\frac{1}{N_i}\right]^{1/3} \qquad (1.2)$$

$$\text{(iii) Polaron radius } r_p\ (\text{Å}) = \frac{1}{2}\left[\frac{\pi}{6N_i}\right]^{1/3} \qquad (1.3)$$

The field strength (F_i) of transition metal ion in the glass matrix is described through the oxidation number (z) and the ionic radii (r_p) of the transition metal ions by:

$$\text{(iv)}\quad \text{Field strength } F_i\ (\text{cm}^{-2}) = \frac{z}{r_p^{\,2}} \qquad (1.4)$$

1.2.2 *Dielectric properties*

When an insulating glass (a dielectric) like $PbO\text{-}Sb_2O_3\text{-}As_2O_3$ glass ceramic is placed in external electric field two types of polarizations – the electronic and the ionic – are expected to develop in the glass ceramic. If the dielectric contains permanent dipoles, they experience a torque in an applied field that tends to orient them in the field direction. Consequently, an orientational (or dipolar) polarization can arise. These three polarizations are due to charges locally bound in atoms, molecules or in the structures of solids. Additionally to all these, generally there exist charge carriers that can migrate for some distance through the dielectric. Such charge carriers during

their motion may be trapped in the material or on interfaces (because they cannot be freely discharged or replaced at the electrodes); due to these causes, space charges and a microscopic field distortion result. Such a distortion appears as an increase in the capacitance of the sample and may be indistinguishable from a real rise of the dielectric constant. Thus a fourth polarization, called the space charge polarization comes into play. The total polarization is sum of these four polarizations (assuming that they act independently) [47].

When the dielectric is placed in alternating fields, these polarizations are set up and the dielectric constant is a consequence of them; also a temporal phase shift is found to occur between the applied field and the resulting polarization and a loss current component appears, giving rise to the dielectric loss of the sample [48].

The complex dielectric constant, according to Debye for a material having permanent dipoles characterized by single relaxation time τ, given by:

$$\varepsilon^* = \varepsilon_\infty + \frac{\varepsilon_s - \varepsilon_\infty}{1 + i\omega\tau} \qquad (1.5)$$

Where, ε_s is the static dielectric constant and ε_∞ is the dielectric constant value of the material corresponding to its electronic and atomic polarization. Separating this equation into its real and imaginary parts, one obtains:

$$\varepsilon'(\omega) = \frac{\varepsilon_s - \varepsilon_\infty}{1 + \omega^2\tau^2} \tag{1.6}$$

and

$$\varepsilon''(\omega) = \frac{(\varepsilon_s - \varepsilon_\infty)\omega\tau}{1 + \omega^2\tau^2} \tag{1.7}$$

The dielectric loss of the material (generally expressed by tan δ) is given by the expression:

$$\varepsilon''(\omega) = \frac{(\varepsilon_s - \varepsilon_\infty)\omega\tau}{1 + \omega^2\tau^2} \tag{1.8}$$

If the conductivity (σ_{ac}) of the sample is also taken into account, it can be shown that $Tan\delta = \frac{4\pi\sigma}{\omega\varepsilon'(\omega)} + \frac{(\varepsilon_s - \varepsilon_\infty)\omega\tau}{\varepsilon_s + \varepsilon_\infty\omega^2\tau^2}$ (1.9)

By plotting log (tan δ) as a function of log (ω), information regarding d.c conductivity as well as the behaviour of the dipoles present if any can be obtained.

1.2.3 *Optical absorption*

Optical radiation interacts with materials in a variety of ways depending upon the material and the wavelength of the optical radiation-giving rise to the optical spectra, which could be either emission or

absorption spectra in solids, normally it is the absorption spectra, which is observed. This is nothing but the variation of the radiation intensity as a function of wavelength. Study of the absorption spectra of transition metal ions embedded in solids had been extensively used to obtain information about the local symmetry in which the ion sits in its valence state, its site preference and determination of the degree of covalency of the metal-ligand bond. When a transition metal ion is embedded in a glass it need not have a centre of symmetry. This leads to mixing of d- and p- orbitals of the ion and, therefore, an electronic transition involves some charge transfer from a d-orbital to a p-orbital leading to weak absorption bands. If an ion is at the centre of symmetry, such a mixing does not occur but during the inevitable molecular vibrations make an ion spend part of the time away from the equilibrium position, which enables mixing of d- and p-orbitals and allow such transitions.

Most of the physical properties of the transition metal complexes are studied with the help of crystal field, ligand field and molecular orbital theories. The ligand field theory explains the optical levels by energy splitting of the states of the central ion in the field of the surrounding atoms. The theory of this splitting under the influence of fields produced by various symmetries has been worked out recently [49-51]. The principal symmetry

of the transition metal complexes is usually an octahedral one while in a few cases, tetrahedral, square planar and lower symmetries occur. In a complex the site symmetry of anions is always degraded from the extremely high spherical one to a lower symmetry. Two types of symmetries, known as octahedral (designated by O_h) and tetrahedral (designated by T_d) are important. The corresponding molecular structures having these symmetries are shown diagrammatically in Fig. 1.7.

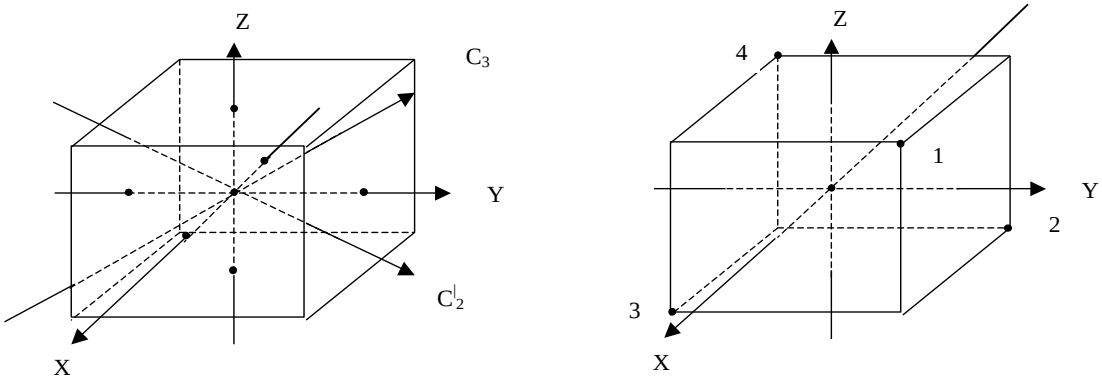

Fig. 1.7 (a) Regular Octahedron point group (O_h)
(b) Regular Tetrahedron point group (T_d)

A free d-electron has five-fold degeneracy with all the five d-orbitals, namely d_{xy}, d_{yz}, d_{zx}, d_x^2-$_y^2$ and d_z^2 possessing the same energy (Fig.1.8a). In a weak field approach, one tries to understand the effect of crystal fields on the free ion terms. In a weak field approach, one tries to understand the effect of crystal fields on the free ion terms (Fig. 1.8 b, c, d).

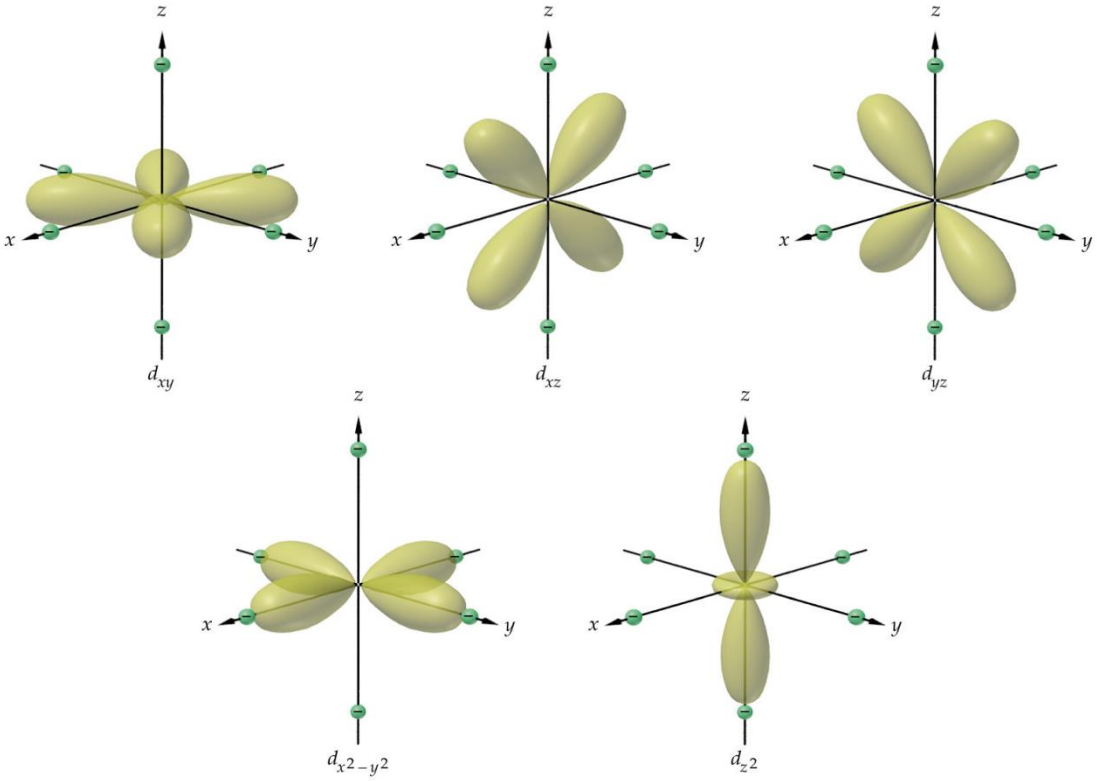
z
x
y
d_{xy}
z
x
y
d_{xz}
z
x
y
d_{yz}
z
x
y
$d_{x^2-y^2}$
z
x
y
d_{z^2}

Fig. 1.8 (a) Five d orbitals of T_{2g} orbitals and e_g orbitals.

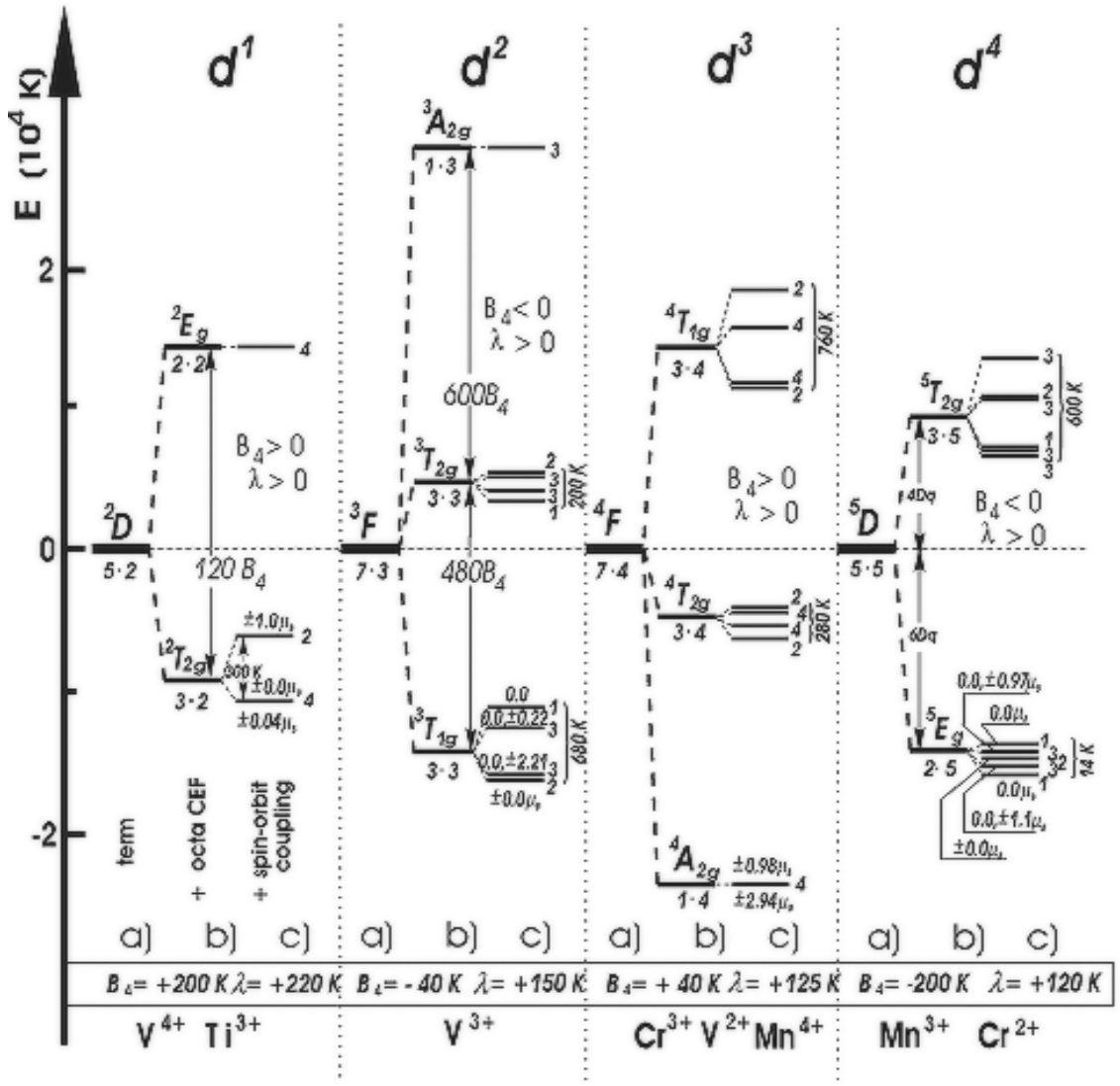

Fig. 1.8 (b) Detailed spectral information on various transition metal (from d^1 to d^4) ions.

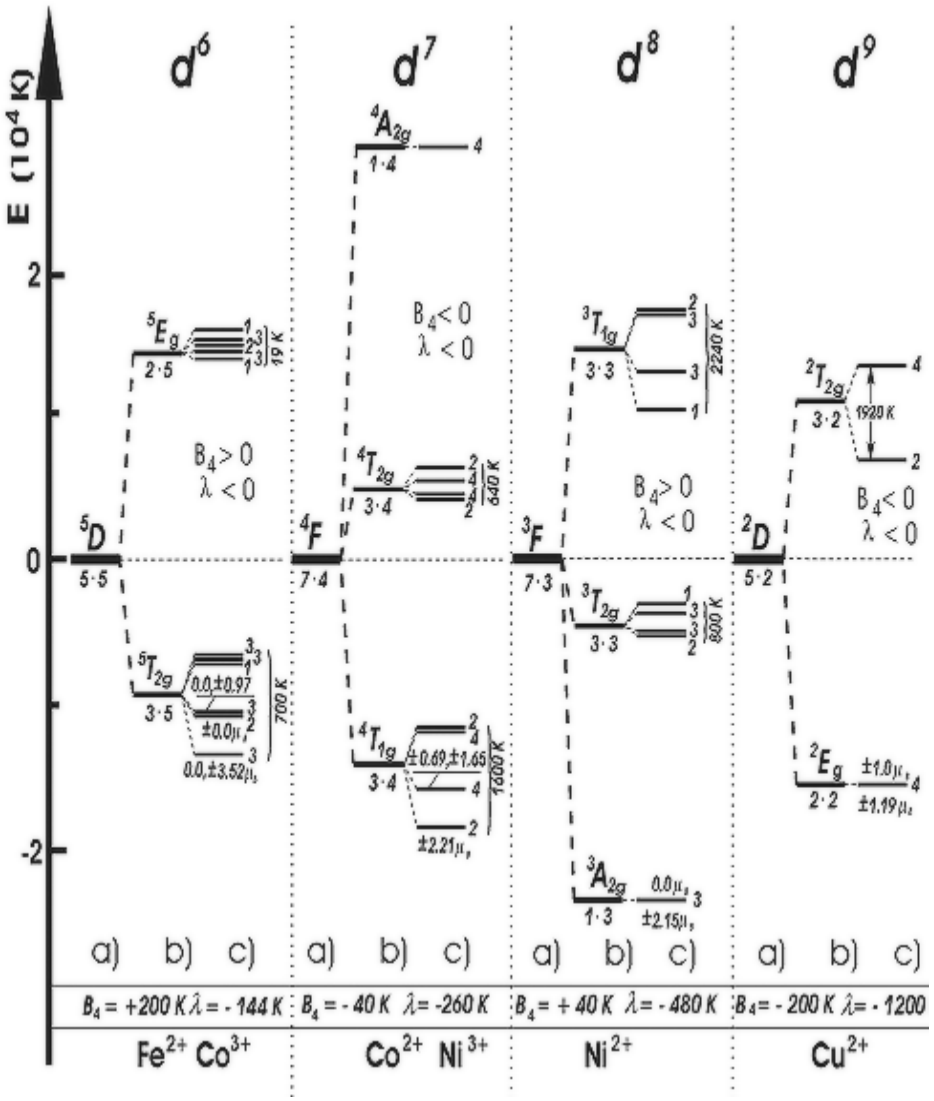

Fig. 1.8 (c) Detailed spectral information on various transition metal (from d^6 to d^9) ions

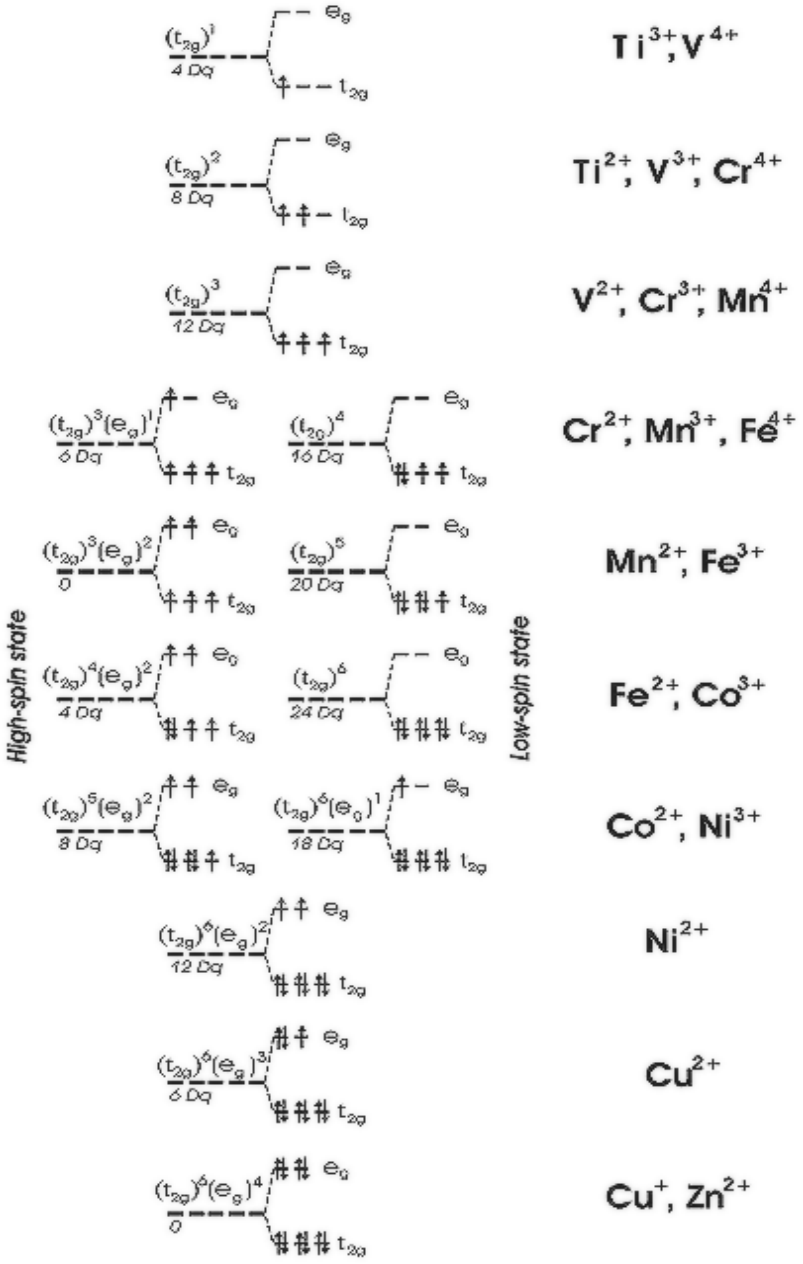

Fig. 1.8 (d) Energy spectra of transition metal ions.

For d case, the application of the group theory results in the splitting of ^2D state into e_g and t_{2g} representations in octahedral crystal field. The crystal field potential acting on the ion is given by

$$V_{oct} = D(x^4+y^4+z^4-(3/5)r^4) \quad (1.10)$$

where $D = (Ze/4a^5)$. This potential has to be applied on the wave functions which transform as t_{2g} whereas $d_{x^2-y^2}$ and d_{z^2} transform as e_g, and

$$<t_{2g}/V_{oct}/t_{2g}> = - 4D_q \quad (1.11)$$

$$<e_g/V_{oct}/e_g> = 6D_q \quad (1.12)$$

Thus, the separation to D_q between t_{2g} and e_g levels is a measure of the crystal field. The centre of gravity of the levels is preserved after application of the crystal field potential.

In tetrahedral (T_d) symmetry, the nature of the splitting is the same but ordering of the levels is inverted as shown in Fig. 1.9. If the symmetry is lower than octahedral, say tetragonal or orthorhombic, then these levels will split into levels of lesser degeneracy. The above discussion is valid for single electron d orbitals. Similar procedure is adopted for multi electron system where the terms will be split into various irreducible representations.

In the case of strong octahedral crystal fields, the single electron t_{2g} and e_g functions become the basis. The various configurations many electron systems are obtained by filling the t_{2g} shell first and then the e_g shell. Thus for

example, the d^2 ion has t_{2g}^2, $t_{2g}^1.e_g^1$ and e_g^2 configurations with energies - $8D_q$, $2D_q$ and $12D_q$, respectively.

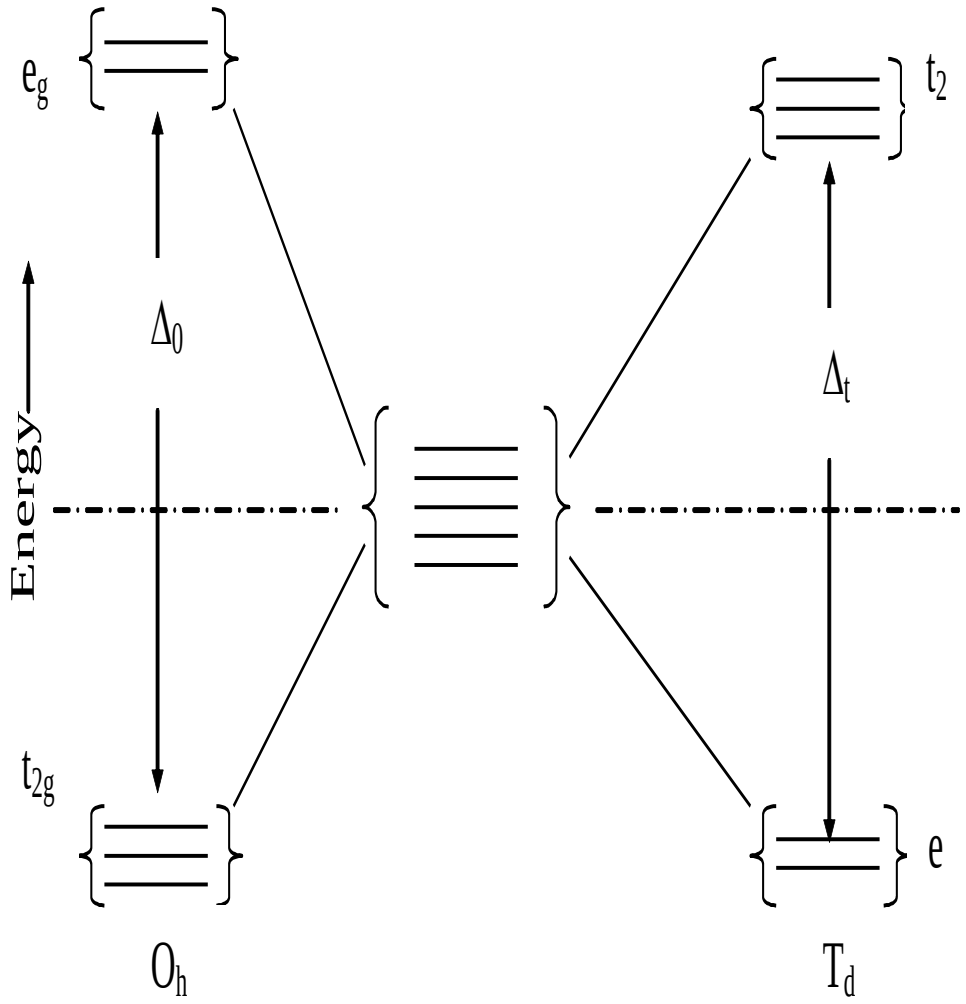

Fig. 1.9 Diagram showing relative energy of e_g and T_{2g} orbitals resulting fro splitting of d orbitals by octahedral environments.

The electrostatic energy values for different states have been calculated by Tanabe and Sugano [52] and Griffith [53] and they have presented these energy values in the form of matrices. For convenient interpretation of the observed optical spectra, Tanabe and Sugano have drawn energy level diagrams between E/B and D_q/B for various d^n configurations known as Tanabe-Sugano diagrams. Here, E corresponds to the energy level of a d^n system and B is the Racah inter-electronic repulsion parameter. These diagrams are mainly used in crystal field spectroscopy to evaluate the crystal field parameter D_q and parameters B and C. From these diagrams, it is possible to obtain a quantitative measure of the ease of spin pairing. These diagrams also help in assigning the transitions correctly.

1.2.4 *Electron spin resonance*

Electron spin resonance (ESR) has been developed as an extremely sensitive and important spectroscopy technique, which is widely used to study systems having unpaired electrons. In condensed matter physics, ESR is used as a powerful technique to study the lowest energy levels, hence, the electronic state of the unpaired electrons of paramagnetic species in solids. This technique provides information on understanding of the symmetry of the surroundings of the paramagnetic ion and the nature of

its bonding to the nearest diamagnetic neighbors. Following are a few examples of systems containing unpaired electrons.

1. Atoms having odd number of electrons, e.g., atomic hydrogen and lithium atom.
2. Molecules with odd number of electrons such as NO, and triplet state molecules like oxygen molecule.
3. Ions having partially filled inner electronic shells, e.g., iron, rare earth ions etc.
4. Defects produced in a solid by irradiation.
5. Free radicals, e.g., CH_3 and diphenyl-picrylhydrazyl.
6. Conduction electrons in metals, semiconductors and dilute alloys etc.

When a system having non-zero angular momentum and magnetic moment is placed in an external magnetic field, each degenerate electronic level splits into a number of levels depending upon the value of angular momentum (Zeeman splitting). The ESR technique, basically, is the observation of the transitions induced by an electromagnetic radiation of appropriate polarization and energy (frequency) between these Zeeman levels. The energy separation of these levels is typically of the order of 1 cm^{-}

[1] (microwave frequency range) in atomic and molecular systems. Thus, a microwave spectrometer is normally required to observe ESR.

An electron possesses spin and associated with it is the spin angular momentum "S" in units of ħ. An electron in a system like an atom or ion will also have, in general, an angular momentum "L" in units of ħ. The total angular momentum "J" is then given by

$$\vec{J} = \vec{L} + \vec{S}. \qquad (1.13)$$

Associated with the total angular momentum J, the magnetic dipole moment μ given by

$$\vec{\mu} = -g\beta \vec{J} \qquad (1.14)$$

where

$$g = 1 + \frac{J(J+1) + S(S+1) - L(L+1)}{2J(J+1)} \qquad (1.15)$$

which is known as the Lande splitting factor for free ion and

$$\beta = \frac{e\hbar}{2mc} = 9.274096 \text{ X } 10^{-27} \text{ erg/gauss} \qquad (1.16)$$

which is known as the Bohr magneton. When a magnetic dipole is placed in a uniform magnetic field B, it precesses about the direction of B with the Larmor angular frequency ω_L which is given by [54]

$$\omega_L = \gamma B \qquad (1.17)$$

where $\gamma = g \beta / \hbar$ is known as gyromagnetic ratio. Thus, the resonance condition will be satisfied only when the frequency of the incident radiation is given by

$$h\nu = g \beta B. \qquad (1.18)$$

When an electromagnetic radiation of a frequency ν is applied to the sample, the resonant absorption of the energy by the unpaired electrons in the sample takes place whenever the resonance condition is satisfied.

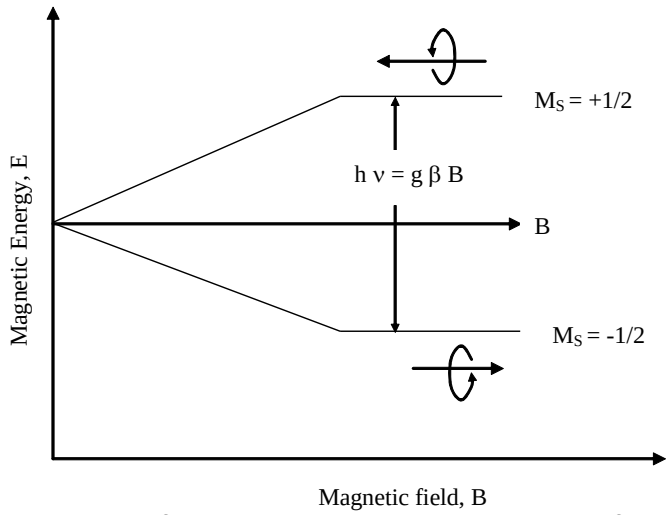

Fig. 1.10 Zeeman energy for a single unpaired electron as function of magnetic field B. A magnetic dipole aligned parallel to B has lower energy while a magnetic dipole aligned antiparallel to B has higher energy.

The energy level of an electron with total angular momentum J has a degeneracy of (2J + 1). The application of an external magnetic field removes this degeneracy and the energy level splits into (2J + 1) levels. When angular momentum L is zero then J becomes equal to S. The transitions between these levels are governed by the selection rules $\Delta M_s = \pm 1$, where M_s is the spin magnetic quantum number. An unpaired electron with $S = \pm 1/2$, when placed in a uniform magnetic field B, will have two energy levels, as shown in Fig. 1.10, if g is constant. The energies of these levels are

$$E_{\pm 1/2} = \pm(1/2) g \beta B, \qquad (1.19)$$

and the energy difference between the two levels for a given value of B is

$$\Delta E = g \beta B \qquad (1.20)$$

The above equation shows that the energy difference between the two levels increases linearly with B in the ESR technique. The magnetic dipole transitions between the levels are induced between the two levels in the presence of a uniform magnetic field B and an alternating magnetic field polarized perpendicular to B by an incident radiation of frequency ν if the quantum condition (1.18) and $\Delta M_s = \pm 1$ are satisfied. This will give rise to only one absorption line. When the orbital angular momentum is not zero then the degenerate energy level will split into (2J+1) levels and the

conditions for the transitions by absorption of energy is given by eqn. (1.18) and $\Delta M_J = \pm 1$. Such a situation will give rise to multiple absorption lines. The resonance condition (1.18) can be satisfied either by changing the magnetic field or the frequency of the radiation incident on the magnetic dipole. Practically, it is more convenient to vary the uniform magnetic field rather than the frequency of the incident radiation since the frequency variation of a microwave source is possible within a very small range only.

Thus, from an ESR spectrum recording one can get information about the resonance field at a fixed frequency of the electromagnetic radiation, hence, the 'g' value, the shape, amplitude and width of the absorption line. The 'g' value may be modified by the crystal field surrounding the free ion from the value of the "free ion value". All of these parameters, when interpreted properly and in conjunction with the appropriate theoretical ideas, provide valuable information on the system studied. In addition, one may vary certain other external parameters like temperature, composition etc., which would possibly change ESR parameters leading to additional information on the system under study. A vast discussion on ESR technique and its applications is available in a number of pioneering books written by many authors [55-59].

a) General Spin- Hamiltonian

In ESR spectroscopy, the transitions can be observed between the energy levels of ground state. In order to get the eigen values and eigen functions, we need to solve the Schrödinger's time- dependent equation applied on Hamiltonian operator. For a Hamiltonian consisting of more than one term, the easier way to solve the equation is by perturbation theory. Here the eigen value is found by taking the strongest interaction and then the next interaction will be treated as a perturbation of the levels obtained in the first case. This procedure is repeated until the weakest interaction is included. This method suffers with a draw back that various interactions should differ from one another by at least one or two orders of magnitude. Incidentally, this condition is satisfied in EPR spectroscopy.

The Hamiltonian, which describes various interactions of unpaired electrons with the static magnetic field and that of the surrounding environment, can be formalized in terms of spin operators. The coefficient of spin operators is called spin-Hamiltonian parameters.

The concept of Hamiltonian was originally developed by Pryce [60] and Abragam and Pryce [61] to interpret the observed resonance of ions in the first transition series. The concept was subsequently extended by Elliott and Stevens [62] to interpret the paramagnetic behavior observed for the rare

earth ions. The terms in the general Hamiltonian for an ion in a crystalline environment can be written as [63].

$$H = H_E + H_{LS} + H_{SI} + H_Q + H_V + H_{SH} + H_{lH} \quad (1.21)$$

Where the symbols indicate the type of interaction to which Hamiltonian applies and have the following meaning.

i. H_E is a composite term expressing the total energy of electrons, the columbic attractions of the electrons and the nuclei and the repulsion among the electrons

ii. $$H_E = \sum_i \left[\frac{P_i^2}{2m} - \frac{Ze^2}{r_i} \right] + \sum_{ij} \frac{e^2}{r_{ij}} \quad (1.22)$$

Where P_i is the momentum of i^{th} electron, r_i is the distance of the electron from the nucleus, r_{ij} is the distance between the i^{th} electron and j^{th} electron and Ze is the nuclear charge.

These terms are summed over all the electrons and yield the unperturbed electronic levels before considering the interaction between spin and orbital angular momenta. The separations will be of the order 10^5 cm^{-1}.

iii. H_{LS} represents the spin-orbit coupling and may be written in the form.

$$H_{LS} = \sum \lambda_{ij} \bullet l_i \bullet s \quad (1.23)$$

Where l is the orbital angular momentum of the individual electron, 's' is the spin angular momentum of the individual electron and λ_{ij} is the spin – orbit coupling constant. This can be written in a simple form as

$$H_{LS} = \lambda \ \mathrm{L} \bullet S \qquad (1.24)$$

Where, L and S are the total orbital angular momentum and the spin angular momentum of free ion respectively. The magnitude of this interaction lies in the range 10^2 to 10^3 cm^{-1}.

iv. H_{SI} describes the magnetic interaction between each electron and the nucleus

$$H_{SI} = \sum \ a_i \bullet \mathbf{J}_i \bullet \mathbf{I}_i \qquad (1.25)$$

Where $\mathbf{J}_i$ is the total angular momentum of the i^{th} electron and $\mathbf{I}_i$ is the nuclear spin. The magnitude of this interaction will be of the order of 10^{-2} cm^{-1}.

v. H_Q represents the nuclear quadrupole interactions, which are even smaller than H_{SI} (~ 10^{-4} cm^{-1}) and may be neglected. For nuclei with spin **I** > ½, these interactions shift the hyperfine levels by a small amount.

$$H_Q = \sum \ \mathbf{I}_i \bullet \ \mathbf{Q}_i \ \bullet \ \mathbf{I}_i \qquad (1.26)$$

vi. H_v represents the effect of crystal field, which can be written as

$$H_v = \sum e_i \ \mathbf{V}(r_i) \qquad (1.27)$$

Where $\mathbf{V}(r_i)$ is the electrostatic potential at the ion with which each electron interacts.

In an external magnetic field B, the terms H_{SH} and H_{IH} must be added to represent the interaction of the angular momentum of electrons and nuclei respectively with the magnetic field.

$$H_{SH} = \beta \ (\mathbf{L} + g_e \ \mathbf{S}) \ . \ \mathbf{B} \qquad (1.28)$$

$$H_{IH} = \mathbf{h} / 2\pi \sum_i -\gamma_i \ . \ \mathbf{I}_i \ . \mathbf{B} \qquad (1.29)$$

Where γ_i is the gyrometric ratio of the i^{th} nucleus and the latter terms (about 10^{-4} cm^{-1}) may be neglected expect in considering second order effects in the nuclear hyperfine interaction.

b) Line shapes

The most commonly observed shape functions in EPR spectroscopy are Lorentzian and Gaussian, described by the functions given below.

$$\mathbf{I} = \frac{I_0}{T_2^2 (B - B_r)^2 + 1} \qquad (1.30)$$

$$\mathbf{I} = I_0 \exp [-b \ (B-B_r)^2 \ T_2^2] \qquad (1.31)$$

Where I_0 is the intensity of the absorption at its centre, B_r is the resonant field at the line centre. The constants T_2^2 and b are related to the half width of each of the two types of curves.

The Lorentzian shape arises due to harmonically bound electron. If the harmonic motion of the electron is interrupted by some process, then the distribution of frequencies follow the equn. (1.31) for an EPR spectrum, the interruption will be in the form of exchange. Since all the electrons are equivalent, their interchanging between two molecules is quite possible if the molecules are close enough to each other. If this exchange is so rapid to affect the phase coherence of the spins, Lorentzian shape results.

On the other hand, Gaussian shape results from the paramagnetic ion separated from each other by molecules, which are having no unpaired electrons but possessing magnetic nuclei. Each unpaired electron will experience a local static magnetic field which will be dominated by how the nuclear spins are arranged in the near by host molecules. The observed EPR spectra will be a superposition of shapes from all the spins with their local fields. Since the local fields will be randomly distributed, the total line shape results in a Gaussian line shape according to equn (1.30). The characteristic Lorentzian and Gaussian line shape are shown in the Fig. 1.11.

c) Line Width and Intensities

Generally the EPR signals are recorded as the first derivative of the absorption curve and hence the area under the EPR signal can be calculated by numerical double integration method. In this method, the EPR spectrum is

divided in to ‘n’ small intervals having length‘d’. The height hr of the EPR signal corresponding to the centre of r^{th} interval is noted and the area under the curve can be calculated from the equation

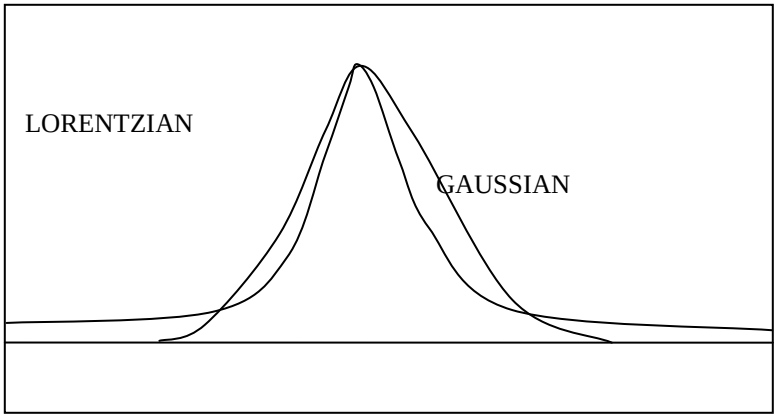

Fig. 1.11 The characteristic Lorentzian and Gaussian line shapes.

$$\mathbf{A} = \mathbf{1/2}\ d^2 \sum_{r=1}^{n} (n - 2r + 1)\ h_r \qquad (1.32)$$

Fig. 1.12 shows the method of finding the area under the first derivative absorption curve by numerical double integration method. The accuracy of this method depends on the number of intervals and complexity of the spectrum. Using about 8 to 10 intervals per peak, the error in calculating the area will likely be within 2 to 3% in Gaussian curves. For Lorentzian curves, the error may be greater due to the presence of long tails.

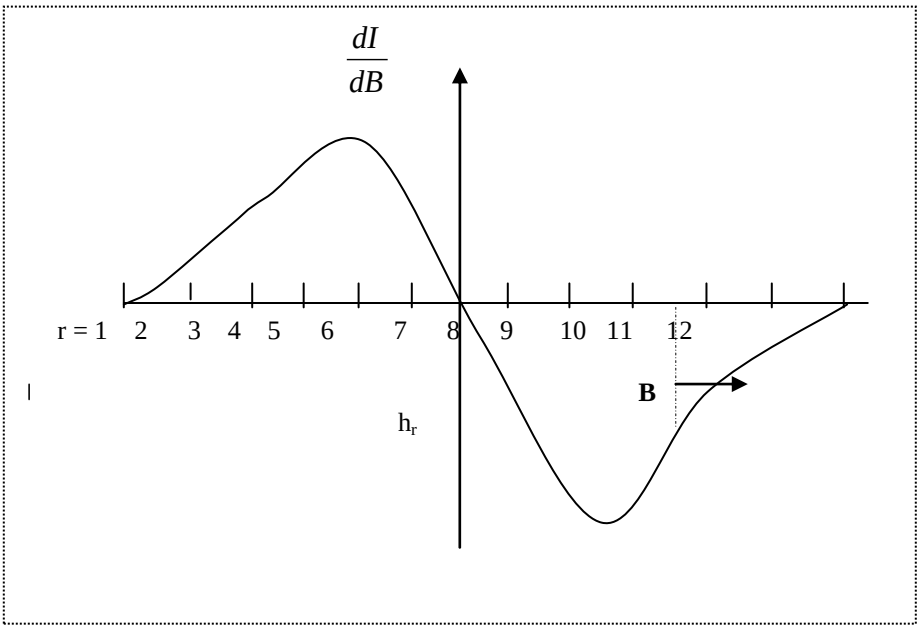

Fig. 1.12 The method of finding the area under the first derivative absorption curve by numerical double integration method.

For ESR signals, the line widths are measured from the maximum and minimum line positions at the first derivative curve. The ESR lines always have a finite width due to electrons interacting magnetically with the environment of the sample. Hence, from the line width and the rate of build up or decay of the line intensity, one can obtain information about spin environment.

The intensity of ESR signals depends on various factors: (1) concentration of the paramagnetic ion, (2) the microwave frequency, (3) the power of microwaves, (4) the transition probability and (5) the temperature.

1.2.5 *Magnetic susceptibility*

Many compounds of the transition elements are paramagnetic, because they contain partially filled electron shells. If the magnetic moment is measured, the number of unpaired electrons can be calculated. The magnetochemistry of the transition elements shows whether the d electrons are paired. This is of great importance in distinguishing between high spin and low spin octahedral complexes. Thus, the magnetic moment μ of a transition metal ion can give important information about the number of unpaired electrons present in the ion and the orbital that are occupied, and sometimes indicates the structure of the molecule or complex.

The magnetic susceptibility measurements were under taken with a view to evaluate magnetic moments of the transition metal ions there by knowing whether these ions are in the tetrahedral or octahedral positions. The susceptibility of the transition metal ions doped $PbO\text{-}Sb_2O_3\text{-}As_2O_3$ glass powders were measured at room temperature using Guoy's balance. From the paramagnetic susceptibility χ, the magnetic moment μ is determined using the relation,

$$\chi = N\mu^2/3KT. \qquad (1.33)$$

Here, N is the concentration of the paramagnetic ions, K is the Boltzmann constant and T is the temperature in Kelvin scale.

1.2.6 *Infrared spectra*

Infrared absorption spectra of glass ceramics can provide significant and valuable information on the arrangement of atoms, nature of chemical bonding between them, the changes in the atomic configurations caused by increase or decrease of concentration of glass-forming systems and in general, facilitate the probing of the short-and intermediate range in glass networks.

In addition, the investigation of infrared spectra (IR) of glass ceramics enables the assignment of characteristic frequencies to molecular groups in the glass ceramic and hence correlation of IR absorption bands with different units of vitreous structure. In the case of antimoy arsenate glasses, the basic glass contains AsO_3, AsO_4, SbO_3 and SbO_4 structural units in the glass network and when a cation such as Pb is added, it may reside interstitially. Such information about the changes in the basic glass structure that take place upon the addition of a cation can also be studied from the IR spectra.

The vibrations of structural units in a glass and glass ceramic are independent [64-66], unlike the vibrations of complex ions in a crystalline matrix which are dependent of the vibrations of other groups. In probing the structural units and changes that take place in the network with composition of a ternary glass, infrared spectroscopy lends itself as an effective tool,

because the technique is sensitive to short-range ordering and local interactions.

The assignment of the important IR bands observed in $PbO{-}Sb_2O_3{-}As_2O_3$ glasses and glass ceramics of the present work is in general made by comparison of the data with the bands observed in literature, even though some bands attributions have their support from the theory. However, it is possible to provide quantitative justification from the theoretical calculation in the literature [65] for some of the vibrational frequencies assigned to arsenate, antimony oxide and other transitional ion groups like MoO_4 , MoO_6 etc.

When the characteristic group frequencies arise from the vibrations of pure stretching character or of pure bending nature the wavenumber- $\bar{\nu}$ is to given by the equation

$$\bar{\nu} = \frac{1}{2\pi c}\left(\frac{K}{\mu}\right)^{1/2} \qquad (1.34)$$

where c is the velocity of light, m is the reduced mass of the diatomic or triatomic group, K is the stretching or bending force constant. For certain diatomic and triatomic groups, the force constant was evaluated using various empirical formulae available in the literature [65, 66].

1.4 Brief review of the previous work on As_2O_3 and Sb_2O_3 based glasses

and glass ceramics

The studies on physical properties of $PbO\text{-}Sb_2O_3\text{-}As_2O_3$ glasses and glass ceramics as such, are very few. However, some of the latest reports available on the studies of certain As_2O_3 based glasses and Sb_2O_3 are mentioned below.

Stanescu et al [67] have systematically studied the electrical properties of $V_2O_5\text{-}As_2O_3$ glasses and reported that the conduction in these glasses is due to the small polarons. Ardelean et al [68] have investigated the valence states of manganese ions and their interactions in $MnO\text{-}Bi_2O_3\text{-}PbO\text{-}As_2O_3$ glasses. Yannopoulos et al [69] have studied low energy excitations in non-crystalline arsenic trioxide. These studies indicated that low frequency Raman scattering in the temperature range 300-700 K. Jacob et al [70] have studied the arsenic oxide containing phosphate and borate glasses. Chowdari and Akhter [71] have reported ionic transport studies of $Li_2O\text{-}As_2O_3$ glasses. Dutta et al [72] have investigated a.c. conduction mechanism in $SiO_2\text{-}As_2O_3$ glasses; a.c. conduction mechanism in these glasses is shown to arise from a correlated-barrier-hoping model involving bipolarons. They have explained, the variation of frequency exponent ‘s’ qualitatively on the basis of the overlapping large polaron model. They have also observed an anomaly in the dielectric permittivity of the glasses in the temperature range 275-325 K.

Brahma et al [73] have reported transport properties of $BaO-Fe_2O_3-B_2O_3-As_2O_3$ semiconducting glass system.

Prasad and Rambabu [74] prepared glasses of the system $AgI-Ag_2O-As_2O_3$ by different methods and studied the effect of preparation on the conductivity and its correlation with surface analysis using scanning electron microscopy (characterized by studying their transport and surface properties). Culea [75] has studied and discussed some parameters of the electrical conductivity of $V_2O_5-As_2O_3$ glasses and analyzed the experimental data using a computational programme. Nasssau et al [76] have studied arsenic containing heavy metal oxide glasses and reported glass and crystallization temperatures, thermal expansion coefficients and refractive indices of $As_2O_3-Sb_2O_3-TiO_2$ glasses. There have been various reports on arsenate glasses combined with alkali and alkaline earth [77] or with GeO_2 and other oxides [78]. Oyamada et al [79] have studied optical absorption spectra of Ni^{2+} ions and IR spectra in $PbO-GeO_2$ glasses containing As_2O_3. Satyanarayana et al [80] have reported a.c. conductivity studies on the silver molybdo arsenate glassy system. Miller et al [81] have studied arsenic containing $PbO-Bi_2O_3$ glasses and concluded that exceptionally high Raman intensities can be observed in these glasses. Nicula et al [82] have studied the ESR spectra, magnetic susceptibility and electron microscopy of $V_2O_5-As_2O_3$

glasses and correlated the magnetic data with previously reported electrical data.

Som et. al [83] have reported the structure and properties of antimony glasses in the K_2O-B_2O_3-Sb_2O_3-ZnO system and they found that these glasses posses low phonon energy of around 600 cm^{-1}. Their results suggested that with increase in Sb_2O_3 content, the covalent character increases. They have also studied the green and red fluorescence upconversion of neodymium ions in these glasses [84]. Satyanarayana et. al [85] have studied various physical properties viz., non-linear optical properties, dielectric properties over a range of frequency and temperature, optical absorption, electron spin resonance (ESR) of PbO-Sb_2O_3-B_2O_3: CoO glass-ceramics. In this study, the authors have thrown some light on the suitability of these glass ceramics for NLO devices. Zhang [86] et al have investigated the influence of addition of Sb_2O_3 on the properties of low-melting ZnO–P_2O_5 glasses. They summarized that Sb_2O_3 could participate in the glass network and thermal stability of the glasses decreased with increasing Sb_2O_3 content. Gomez et. al [87] have studied nonlinear optical properties of antimony oxide based glasses with excitation wavelengths ranging from 800 to 1600 m. They have evaluated NL refractive indices, n_2, and the two-photon absorption (TPA) coefficient, beta, using the Z-scan

technique. Dovzhik [88] have studied the electrical properties of films of TeO_2-Sb_2O_3 glasses. Wood [89] have investigated the influence of antimony oxide on the structure of alkaline-earth alumino borosilicate glasses. Bosco et. al [90] have reported ultrafast nonlinearity of antimony polyphosphate glasses by Kerr shutter technique. They have concluded that with the addition of 10% of lead oxide in the glass composition, the nonlinear refractive index n_2 is increased by 80%. Takahiro et al [91] have studied the effect of antimony oxide on the deposition and dispersion of metallic copper nanoparticles in phosphate glasses. Tsuyoshi et al [92] have reported the results of XPS study of antimony borate glasses. Amano et al [93] have investigated the electrical properties of Sb_2O_3–CaO–V_2O_5 glasses and glass-ceramics. Ghosh [94] reported the DC conductivity of the semiconducting vanadium tellurite glasses containing Sb_2O_3 in the temperature range 80-500 K and he interpreted the results in terms of polaron-hopping theories. Lüdersdorf et al [95] have reported the biological assessment of exposure to antimony and lead in the glass-producing industry. Chakravorty et al [96] have measured DC and AC resistivities of some oxide glasses containing antimony oxide. On the basis of chemical analysis and DTA studies, they have shown that at temperatures below 35 ^oC, the conductivity arises due to the presence of both Sb^{5+} and Sb^{3+} ions in the glass system. Parke et. al [97]

have reported the optical properties of Sn^{2+} and Sb^{3+} in calcium metaphosphate glass.

Poirier et al [98] had reported glass formation region for certain ternary antimonyoxide based glasses. They have also carried out the optical transmission and thermal expansion studies on these glasses. Nalin et al [99] have investigated Sb_2O_3–WO_3-$Sb(PO_3)_3$ differential scanning calorimetric and optical transmission studies and have concluded that these glasses have potential photonic applications. Tandon and Hotchandani [100] have reported electrical conductivity of Sb_2O_3-WO_3-TeO_2 glass systems. Recently, Sudarshan and Kulshreshtha [101] have reported the structural aspects of PbO-P_2O_5-Sb_2O_3 glasses. Muruganandam and Seshasayee [102] have reported the structural studies on Li_2O-P_2O_5-Sb_2O_3 glass systems. Datta et al [103] have studied the electrical conductivity of P_2O_5-Sb_2O_3 glasses and have concluded that the conduction in the glasses arises due to the hopping of electron between Sb^{3+} and Sb^{5+} cations. Ghosh and Chaudhuri [104] have reported that addition of Sb_2O_3 to V_2O_5–P_2O_5 glasses makes them stable against moisture. Soltani et al [105] have investigated the glass formation of some new alkali antimonate glasses. Legouera et al [106] have reported the glass formation in the Sb_2O_3-$ZnBr_2$ binary system. Ardelean et al [107] have studied the magnetic properties of Fe_2O_3-Sb_2O_3-TeO_2 glasses. Hong–Hua et

al [108] have studied the conductivity and high effective dielectric constant Fe_2O_3-Sb_2O_3-TeO_2 glasses. De Vicente et al [109] have reported the photo induced structural changes in antimony poly phosphate based glasses. Raghavaiah et al [110] have studied the thermoluminescence of lead antimony arsenate glasses doped with iron ions. They also investigated the optical and magnetic properties of these glasses containing vanadium ions [111].

In spite of these studies still there is a lot of scope to investigate on $PbO{-}Sb_2O_3{-}As_2O_3$ glasses and glass ceramics mixed with different transitional ions especially on dielectric properties and other related properties.

1.5 Motivation and objective of the present work

Heavy metal oxide based glass ceramics like $PbO{-}Sb_2O_3$ have attracted an enhanced interest in recent years. These materials posses large nonlinear optical susceptibility (χ^3) coefficient, that makes them suitable for potential applications in non-linear optical devices (such as optical switchers, limiters etc.), broad band optical amplifiers operating around 1.5 μm and in a number of solid state ionic devices. Antimony oxide participates in the glass network with SbO_3 structural units and can be viewed as tetrahedrons with the oxygen situated at three corners and a lone pair of electrons of antimony

(Sb^{3+}) at the fourth corner localized in the third equatorial direction of Sb atom. Sb_2O_3 based glass ceramics exhibit significant transparency in the far infrared region and possess high refractive index.

The antimony oxide as mentioned earlier, as such is an incipient glass network former, does not form glass on its own. The addition of As_2O_3 to Sb_2O_3 facilitates glass formation and further there are some common vibration bands at about same frequencies in the infrared region for these oxides and hence there is a possibility for the formation of linkages of the type Sb-O-As. The addition of As_2O_3 to $PbO{-}Sb_2O_3$ glasses is expected to make these glasses useful for low-loss materials for long-distance optical transmission. The glasses containing As_2O_3 have exceptionally high transmission potential in the far-infrared region when compared with the conventional glasses like B_2O_3, SiO_2, P_2O_5 and GeO_2. They possess very high Raman scattering coefficients and found to be suitable for active fiber Raman amplification. Certain studies on As_2O_3 glasses mixed with alkali halides, rare earth oxides and some heavy metal oxides like TeO_2, Bi_2O_3, etc., were reported with narrow glass-forming regions. As_2O_3 is the only strong network former besides GeO_2 that exhibit significant transmission potential farther into the infrared.

The utility of PbO−Sb_2O_3-As_2O_3 glasses can be further enhanced by crystallizing them partially with appropriate nucleating agents. The crystallized glass materials possess small and strain free intertwined crystals that hinder the crack growth. As a result, these materials are expected to possess outstanding physical properties (when compared with amorphous materials) like high mechanical and electrical insulating strengths, high chemical durability and low coefficient of thermal expansion.

Although crystallization with transition metal ions is mostly confined to SiO_2 based glasses, there are a considerable number of recent reports where transition metal ions have been used as nucleating agents and observed to induce phase separation in other glass systems.

Among various transition metal ions, the molybdenum ions are expected to have profound influence on the optical and electrochemical properties of PbO–Sb_2O_3–As_2O_3 glass ceramics, in view of the fact that the oxide of molybdenum participate in the glass network with different structural units like MoO_4 (Td) and MoO_6 (Oh) of Mo^{6+} ions and $Mo^{5+}O^{3-}$ (Oh) of Mo^{5+} ions. The presence of molybdenum ions makes the glasses to be useful for potential applications in high-density memories, light modulation; large area displays devices like smart windows and other electro-chromic devices.

Similarly the inclusion of MnO into the antimony arsenate glass ceramic network is an added advantage to use these materials for optically operated devices, since unfilled d-shells of these ions contribute more strongly to the non-linear polarizabilities. A considerable number of recent studies on a variety of materials with MnO as nucleating agent are available in the literature.

The crystals, glasses containing nickel ions as nucleating agents are considered as good candidates for ultra broad band optical amplifiers that are widely used in telecommunication systems and hence the investigations on NiO mixed PbO-Sb_2O_3-As_2O_3 glass ceramics are expected to give some interesting results which may be helpful for the practical applications of these glasses.

Thus the clear objectives of the present study are to prepare, characterize and

- To have a comprehensive understanding over the influence of molybdenum, manganese and nickel ions on structural aspects of PbO−Sb_2O_3-As_2O_3 glass ceramics by investigating the dielectric properties, optical absorption, luminescence, ESR and IR spectra and to throw some light on the practical utilization of these materials.

1.6 Contents of the present work

The compositions of the glasses used for the present study are

1. 40PbO- (20-x)Sb_2O_3-40As_2O_3: x MoO_3 ($0 \leq x \leq 1.0$)

2. 40PbO- (20-x)Sb_2O_3-40As_2O_3: x MnO ($0 \leq x \leq 5.0$)

3. 40PbO- (20-x)Sb_2O_3-40As_2O_3: x NiO ($0 \leq x \leq 1.0$)

The studies carried out are

(viii) differential thermal analysis and the evaluation of glass transition temperature T_g,

(ix) infrared spectral studies in the wavenumber range 400-2000 cm^{-1} and the study of the effect of concentration of transition metal ions on the position and intensity of various vibrational bands;

(x) optical absorption studies in the wavelength range 300-2100 nm, identification of various electronic transitions of transition metal ions;

(xi) electron spin resonance measurements and the identification of the enviroment and valence states of molybdenum and manganese ions in the glass network;

(xii) luminescence studies of MnO doped PbO−Sb_2O_3−As_2O_3 glass ceramics.

(xiii) magnetic susceptibility studies of all the three series of the glass ceramics and the evaluation of magnetic moments of the nucleating agents (transition metal ions) and there by assessing valence states of these ions in the glass matrix

(xiv) dielectric properties viz., dielectric constant ε^{l}, dielectric loss tan δ and ac conductivity σ_{ac} in the frequency range 10^{2}-10^{5} Hz and in the temperature range 30-250 ^{o}C;

References

1. W.H. Zachariasen, *J. Am. Chem.Soc.*54 (1932) 3841.
2. W. Vogel, *Glass Chemistry* (Springer Verlag, Berlin 1994)
3. S.R. Elliott, *Physics of Amorphous Materials* (Longmann, Essex, 1990).
4. D.E. Polk, *Scripta metall.* 4 (1970) 117.
5. K.J. Rao, *Structural Chemistry of Glasses,* (Elsevier, Amasterdam, 2002).
6. M.D. Ingram, *Phys. Chem. Glasses* 28 (1987) 215.
7. James E Shelby, *Introduction to Science and Technology of Glass Materials* (Royal Society of Chemistry, 2005).
8. N. Vedeanu, O. Cozar, I. Ardelean, B. Lendl, D.A. Magdas, *Vibrational Spectroscopy* 48 (2008) 259.
9. S. Daoudi, L. Bejjit, M. Haddad, M.E. Archidi, A. Chahine, M.Et-tabirou, P. Molinié, *Spectro. Lett*. 40 (2007) 785.
10. G. Murali Krishna, Y. Gandhi and N. Veeraiah, *Phys. Stat. Sol. (a)* 205 (2008) 177.
11. G. Srinivasa Rao and N. Veeraiah, *J. Solid State Chem*.166 (2002) 104.
12. X. Li, X. Wang, D. He, *J. Shi, Mater. Chem*. 18 (2008) 4103.
13. Z.A. Talib, W.M. Daud, E.Z.M. Tarmizi, H.A.A. Sidek, W.M.M. Yunus, *J. Phys. Chem. Solids* 69 (2008) 1969.
14. P.W. McMillan, *Glass Ceramics, 2nd ed.* (Academic Press, New York, 1979).
15. T.J. Headley and R.E. Loehman, *J. Am. Ceram. Soc.* 67 (1984) 620.
16. K. Terashima, T. Hashimoto, T. Uchino, T. Yoko, *J. Ceram. Soc. Japan*. 104 (1996) 1008.

17. M. Nalin, M. Poulain, J.L. Ribeiro, Y. Messaddeq, *J. Non-Cryst. Solids* 284 (2001) 110.

18. Marcelo Nalin, Marcel Poulain, Michel Poulain, Sidney J. L. Ribeiro, Y. Messaddeq, *J. Non-Cryst. Solids* 284 (2001) 117.

19. E. Fargin, A. Berthereau, T. Cardinal, G. Le flem, L. Ducasse, L. Canioni, P. Segonds, L. Sarger, A. Ducasse, *J. Non-Cryst. Solids* 203 (1996) 96.

20. A. Mori, Y. Ohishi, M. Yamada, H. Ono, Y. Nishida, K. Oikawa, S. Sudo, *Proc. O F C 97* (1997) PDI.

21. J.C. Sabadel, P. Armand, D. Cachau-Herreillat, P. Baldeck, O. Doclot, A. Ibanez and E. Philippot, *J. Solid State Chem* .132 (1997) 411.

22. G. Kumar, D. Chakravorty, *J. Phys. D* 15 (1982) 305.

23. B.V.R. Chowdari, S.K. Akhter, *Solid State Ionics* 25 (1987) 109.

24. W. H. Dumbaugh, *Phys. Chem. Glasses* 19 (1978) 121.

25. K. Muruganandam , M. Seshasayee, *Phys. Chem. Glasses*, 40 (1999) 287.

26. L. Zan, J. Zhong, Qirong Luo, *J. Non-Cryst .Solids* 256 (1999) 396.

27. D. Holland, Solid State NMR 26 (2004) 72.

28. G.D. Parkes, *Mellor's Modern Inorganic Chemistry* (Longmans, London, 1967).

29. P.J. Durrant and B. Durrant, *Introduction to Advanced Inorganic Chemistry*, 2 nd ed (Longmans, London, 1970).

30. J.D. Smith and A.F. Trotman Dickenson, *Comprehensive Inorganic Chemistry* (Pergamon, Oxford, 1973).

31. L.R. Maxwell, S.B. Hendricks and L.S. Deming, *J. Chem. Phys*. 5 (1937) 626.

32. G.C. Hampson and J. Stosick, *J. Amer. Chem. Soc*., 60 (1938) 1814.

33. K.A. Becker, K. Plieth, I. Stranski, *Prog. Inorg. Chem*. 4 (1962) 1.

34. F. Perlik, *Czech. J. Phys. B* 28 (1978) 170.

35. A.G. Clare, A.C. Wright, R.N. Sinclair, F.L. Galeener and A.E. Geissberger, *J. Non-Cryst. Solids* 111 (1989) 123.

36. J.R. Jurado and J.F. Novarro, *J. Non-Cryst. Solids* 38 (1980) 365.

37. C.H. Mackenzie Chung, *J. Non-Cryst. Solids* 42 (1980) 365.

38. E. Culea and Al. Nicula, *Solid. State Commun*. 50 (1984) 929.

39. E. Culea, Al. Nicula and I. Bratu, *Phys. Stat. Solidi (a)*, 84 (1984) 17.

40. G. Srinivasarao, N. Veeraiah, *J. Solid State Chem*. 166 (2002) 104.

41. K. Nassau, D.L. Chadwick and A. E. Miller, *J. Non-Cryst .Solids* 93 (1987) 115.

42. A. Bishay, C.Maghrabi, *Phys. Chem. Glasses* 10 (1969) 1.

43. W.T. Carnall, P.R. Fields, K. Rajn, *J. Chem. Phys.* 49 (1968) 4424.

44. F. Auzel, *Spectroscopy of Solid State Lasers* [B. Bibartaro, ed.] (Plenum, New York 1987).

45. G. Guery J.L. Adam, *J. Lumin.* 42 (1988) 132.

46. M.J. Weber and R. Cropp, *J. Non- Cryst. Solids* 4 (1981) 137.

47. P. Butcher, K.J. Hyden, *Phil. Mag*. 36 (1997) 657.

48. B. Tareev, *Physics of Dielectric Materials, (Mir, Moscow*, 1979).

49. B.N. Figgis, M.A. Hitchman, Ligand *Field Theory and its Applications* (Wiley-VCH Verlag GmbH, Berlin, 2000).

50. A. West, A.R. West, *Solid State Chemistry and Its Applications,* (John Wiley & Sons, Berlin, 1991).

51. J.D. Lee, *Concise Inorganic Chemistry*, (Blackwell Science, London, 1999).

52. Y. Tanabe and S. Sugano, *J. Phys. Soc. Japan* 9 (1954) 753.

53. J.S. Griffith, *The Theory of Transition Metal Ions (*Cambridge University Press, London, 1964).

54. R.A. Smith, *Wave Mech. Crystalline Solids (*Chapman and Hall, London, 1969).

55. M. Bersohn and J.C. Baird, *An introduction to Electron Paramagnetic Resonance (*Benjamin Inc, New York 1966).

56. A. Abragam and B. Bleaney, *Electron Paramagnetic Resonance of Transition Ions*, (Claredon Press, Oxford, 1970).

57. C.P. Poole, Electron Spin Resonance: *A Comprehensive Treatise on Experimental Techniques*, (John Wiley, New York 1984).

58. J.R. Pilbrow, *Transition Ion Electron Paramagnetic Resonance*, (Claredon Press, Oxford, 1990).

59. J.A. Weil, J.R. Bolton, J.E. Wertz, *Electron Paramagnetic Resonance Elementary Theory and Practical Applications*, (John Wiley, New York 1994).

60. M.H.L. Pryce, *Proc. Phys. Soc. A* 63 (1950) 25.

61. A. Abragam, M.H.L. Pryce, *Proc. Roy. Soc. A* 205 (1951)135.

62. R.J. Elliot, K.W.H. Stevens, *Proc. Roy. Soc. A* 218 (1953) 553.

63. P.B. Ayscough, *Electron spin resonance in chemistry*, (Methuen, London, 1967).

64. P. Tarte, *Spectrochim. Acta* 18 (1962) 467.

65. P. Tarte, *Physics of Non-Crystalline Solids* (Elsevier, Amsterdam, 1964).

66. R.A. Condrate, *Introduction to Glass Science*, (Plenum, New York, 1972).

67. L. Stanescu, I. Ardelean, M. Culea, *Amorph. Semiconductors* 82 (1982) 157.

68. I. Ardelean, S. Simon, C. Bob, *Mater. Lett*. 39 (1999) 42.

69. S.N. Yannopoulos, G. Fytas, *J. Chem. Phys.*107 (1997) 1341.

70. A. Jacob, C. Marcel, C. Pedrini, *Mater. Sci. Forum* 239 (1997) 283.

71. B.V.R. Chowdari, S. K. Akther, *J. Non-Cryst. Solids* 116 (1990) 16.

72. A. Datta, A.K. Giri, D. Chakravorty, *Phys. Rev. B* 45 (1992) 1222.

73. P. Brahma, S. Mitra, D. Chakravorty, *J. Phys. D* 23 (1990) 706.

74. P.S.S. Prasad, B. Rambabu, *J. Mater. Sci*. 26 (1991) 2451.

75. E. Culea, *phys. stat. sol. (a)* 126 (1991) 159.

76. K. Nassau, D.L. Chadwick, *J. Am. Ceram. Soc*. 66 (1983) 332.

77. M. Imaoka, *Glass Formation Range and Glass Structure, Adv. in Glass. Tech*. (1962) 149.

78. W.H. Grodkiewicz, H.M.O. Brain, G. Zydzik, *J. Non-Cryst. Solids* 44 (1981) 405.

79. R. Oyamada, K. Sumi, *J. Non-Cryst. Solids* 112 (1989) 282.

80. N. Satyanarayana, M. Venkateswarlu, *J. Mater. Sci*. 31 (1996) 5471.

81. A.E. Miller, M.E. Lines, *J. Non-Cryst. Solids* 99 (1988) 289.

82. A.I. Nicula, I. Lupsa, *J. Non-Cryst. Solids* 79 (1986) 325.

83. T. Som, B. Karmakar, *J. Am. Ceram. Soc*., 92 (2009) 2230.

84. T. Som, B. Karmakar, *J. Alloys and Comp*. 476 (2009) 383.

85. T. Satyanarayana, I.V. Kityk, M. Piasecki, P. Bragiel, M.G. Brik, Y. Gandhi and N. Veeraiah, *J.Phys:. Condens. Matter* 21 (2009) 245104.

86. B. Zhang, Q. Chen, L. Song, H. Li and F. Hou, *J. Am.Ceram. Soc*. 91 (2008) 2036.

87. C.B. de Araujo, L.A. Gomez, E.L.F. Filho, D.N. Messias, L. Misoguti, S.C. Zilio, M. Nalin, Y. Messaddeq, *Transparent Optical Networks* 2 (2007) 293.

88. E.I. Vasileva, A.S. Dovzhik, V.S. Tyushev, O.V. Sheludko, *Soviet Phys. J.* 10 (2004) 69.

89. G.J. Wood, S. Prabakar, T.K. Mueller, G.C. Pantano, *J. Non-Cryst. Solids* 349 (2004) 276.

90. E.L. Falcao, C.A.C. Bosco, G.S. Maciel, C.B. Dearaujo, L. H. Acioli, M. Nalin and Y. Messaddeq, *Applied Phys. Lett*. 83 (2003) 1292.

91. M. Takahiro, S. Masanori, F. Yoshifumi and M. Kenji, *J. Japan Inst. Metals* 64 (2000) 15.

92. H. Tsuyoshi, B. Yasuhiko, K. Takayuki, S. Ryuji, V. Demitrov, *Nippon Seramikkusu Kyokai Shuki Shinpojiumu Koen Yokoshu* 12 (1999) 279.

93. M. Amano, K. Suzuki, H. Sakata, *J. Mater. Sci*. 32 (1997) 4325.

94. A. Ghosh, *J. Phys.: Cond. Matter* 5 (1993) 4485.

95. R. Lüdersdorf, A. Fuchs, P. Mayer, G. Skulsuksai and G. Schäcke, *International Archives of Occupational and Environmental Health*, 59 (1987) 469.

96. D. Chakravorty, D. Kumar and G.V.S. Sastry, *J. Phys. D: Appl. Phys*. 12 (1979) 2209.

97. S. Parke and R.S. Webb, *J. Phys. D: Appl. Phys*. 4 (1971) 825.

98. Gael Poirier, Michel Poulain, M. Poulain, *J. Non-Cryst. Solids* 284 (2001) 117.

99. M. Nalin, Marcel Poulain, Michel Poulain, Sidney J.L. Ribeiro, Y. Messaddeq, *J. Non-Cryst. Solids* 284 (2001) 110.

100. R.P. Tandon , S. Hotchandani, *phys. stat. sol.(a)* 185 (2001) 453.

101. V. Sudarsan, S.K. Kulshreshtha, *J. Non-Cryst. Solids* 286 (2001) 99.

102. K. Muruganandam, M. Seshasayee, *Phys. Chem. Glasses* 40 (1999) 287.

103. A. Datta, D. Chakravorty, *Phys. Rev. B* 47 (1993) 16242.

104. A. Ghosh, B.K. Chaudhuri, *J. Non-Cryst. Solids* 103 (1998) 83.

105. M.T. Soltani, A. Boutarfaia, M. Poulain, *J. Phys. Chem. Solids* 64 (2003) 2307.

106. M. Legouera, P. Kostka, M. Poulain, *J. Phys. Chem. Solids 65* (2004) 901.

107. I. Ardelean, Hong-Hua Qiu, H. Sakata, *Mater. Lett.* 32 (1997) 335.

108. Hong-Hua Qiu, H. Mori, H. Sakata, *J. Ceram. Soc.* 103 (1995) 32.

109. F.S. De Vicente, M. Siu Li, M. Nalin, *J. Non-Cryst. Solids* 330 (2003)168.

110. B.V. Raghavaiah, P. Yadgiri Reddy and N. Veeraiah, *Opt. Mater*. 29 (2007) 566.

111. B.V. Raghavaiah, C. Laxmi Kanth, D. Krishna Rao and N. Veeraiah, *Mater. Lett*. 59 (2004) 539.